Weierstraß-Institut

für Angewandte Analysis und Stochastik

Leibniz-Institut im Forschungsverbund Berlin e. V.

Preprint ISSN 2198-5855

On tetrahedralisations of reduced Chazelle polyhedra with interior Steiner points

Hang Si[1], Nadja Goerigk[1]

submitted: December 9, 2015

[1] Weierstrass Institute
Mohrenstr. 39
10117 Berlin
Germany
email: Hang.Si@wias-berlin.de

No. 2190
Berlin 2015

2010 *Mathematics Subject Classification.* 65D18, 68U05, 65M50, 65N50.

Key words and phrases. indecomposable polyhedron, Chazelle polyhedron, Schönhardt polyhedron, Steiner points, tetrahedralisation, edge flip.

Edited by
Weierstraß-Institut für Angewandte Analysis und Stochastik (WIAS)
Leibniz-Institut im Forschungsverbund Berlin e. V.
Mohrenstraße 39
10117 Berlin
Germany

Fax: +49 30 20372-303
E-Mail: preprint@wias-berlin.de
World Wide Web: http://www.wias-berlin.de/

Abstract

The polyhedron constructed by Chazelle, known as *Chazelle polyhedron* [4], is an important example in many partitioning problems. In this paper, we study the problem of tetrahedralising a Chazelle polyhedron without modifying its exterior boundary. It is motivated by a crucial step in 3d finite element mesh generation in which a set of arbitrary boundary constraints (edges or faces) need to be entirely preserved. We first reduce the volume of a Chazelle polyhedron by removing the regions that are tetrahedralisable. This leads to a 3d polyhedron which may not be tetrahedralisable unless extra points, so-called *Steiner points*, are added. We call it a *reduced Chazelle polyhedron*. We define a set of interior Steiner points that ensures the existence of a tetrahedralisation of the reduced Chazelle polyhedron. Our proof uses a natural correspondence that any sequence of edge flips converting one triangulation of a convex polygon into another gives a tetrahedralization of a 3d polyhedron which have the two triangulations as its boundary. Finally, we exhibit a larger family of reduced Chazelle polyhedra which includes the same combinatorial structure of the Schönhardt polyhedron. Our placement of interior Steiner points also applies to tetrahedralise polyhedra in this family.

1 Introduction

A theoretical difficulty in many geometric problems is the existence of 3d *indecomposable polyhedra*, whose interior cannot be decomposed into a set of tetrahedra whose vertices are all of the given polyhedra, such as the well-known Schönhardt polyhedron [15] and some generalisation of it [1, 13, 10]. Meanwhile, it is NP-complete to determine whether a given 3d polyhedron can be tetrahedralised in this way [14]. Although it is known that any indecomposable polyhedra can be tetrahedralised by inserting a certain number of additional points, so-called *Steiner points*, it remains unknown, for an arbitrary 3d polyhedron, how many Steiner points are required and where these Steiner points should be located.

The polyhedron constructed by Chazelle, known as *Chazelle polyhedron* [4], see Figure 1, is an important example in many partitioning problems. A Chazelle polyhedron consists of two sets of line segments that lie on two slightly shifted doubly-ruled hyperbolic surfaces (saddle surfaces). The space between these two saddle surfaces forms an 3d indecomposable polyhedron. The Chazelle polyhedron was initially used to prove a quadratic lower bound

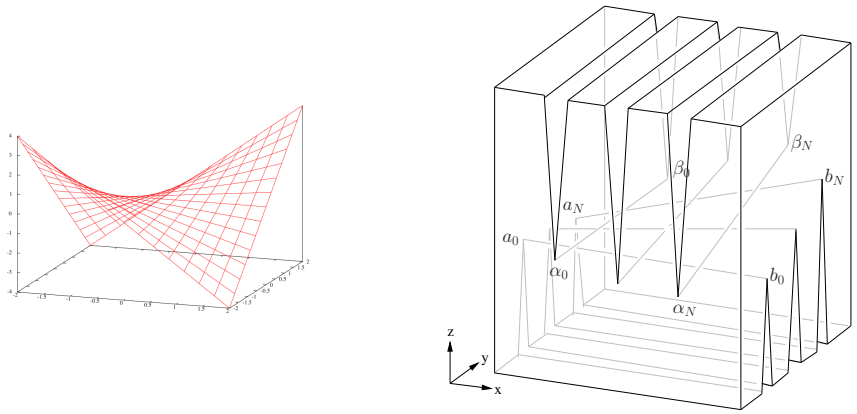

Figure 1 Left: A saddle surface (a hyperbolic paraboloid). Right: The Chazelle polyhedron [4] with three notches, i.e., $N = 2$, on the top and the bottom faces, respectively.

on the complexity of convex decomposition of any 3d polyhedron [4]. It becomes an useful example to construct lower bounds in many other problems, such as the binary space partition problem [12], the hierarchy of bounding volume for collision detection problem [7], the decomposablility of fat-polyhedra [6], and the optimal tetrahedralisation (in terms of size and shape of mesh elements) in finite element mesh generation [3].

Our interest of the Chazelle polyhedron stems from a crucial step in finite element mesh generation – the *boundary recovery problem* [9, 23, 8, 18], in which a given set of *constraints* (edges or faces) must be entirely preserved in the final meshes. Such constraints are required in various purposes, such as to assign boundary conditions, to access the geometric information, to match another partition sharing at the common interface, to generate anisotropic meshes (whose elements all aligned along certain directions), etc.

A classical method to solve this problem is to start with an initial tetrahedralisation, like the Delaunay tetrahedralisation, and then to recover the missing constraints by locally modifying the mesh through a set of *local mesh transformation operations*, such as edge and face flips, vertex insertion and deletion. All these operations take an input of a *cavity* which is a 3d polyhedron formed by the union of a set of existing tetrahedra and return a set of new tetrahedra that fills the interior of the cavity without modifying its outer boundary. The shape of the cavity is a 3d polyhedron which is not necessarily convex. In many cases, the presented cavity has a simple shape so that a missing constraint can be easily recovered by only performing flips. However, if a cavity is an indecomposable polyhedra, interior Steiner points are needed in order to complete the tetrahedralisation process.

Since it is difficult to detect an untetrahedralisable cavity in advance, many heuristics methods are developed. Most of the approaches first try using flips as much as possible, then try adding Steiner points [9], or interchange these two operations [23, 8, 18]. In practice, all these approaches worked very well. Nice results on some rather complicated 3d polyhedra are reported. However, no surprising, they may fail unexpectedly on some special inputs. As an example, we tested two state-of-the-art codes (one commercial, one public domain) on a Chazelle polyhedron with a rather small number of input vertices, both of these codes run much slower compared with other inputs, and produced very different numbers of interior Steiner points. Moreover, when we made the volume of the Chazelle polyhedron slightly smaller, both codes failed to produce a valid output.

A theoretical difficulty in these algorithms is due to the fact that there is a lack of

knowledge about the geometry and combinatorial structures of the whole family of 3d indecomposable polyhedra. There are only few work [11, 2, 22, 7, 6] on these topics. In [10], we proved the optimal number of interior Steiner points for some 3d indecomposable polyhedra whose geometric structures are understood, such as the Schönhardt polyhedron, Bagemihl polyhedron, and a more general class of them. This result provides useful suggestion to design correct and efficient algorithms to tetrahedralise such polyhedra. However, there are still many unknown cases of 3d indecomposable polyhedra. There might not have practically useful answers can be searched for these issues if an arbitrary 3d indecomposable polyhedron is considered. Therefore, it is meaningful to consider these answers for some specific types of indecomposable polyhedra, such as the Chazelle polyhedra.

If Steiner points are allowed to be placed everywhere for a given 3d polyhedron, then there are many solutions. For example, the algorithm of Chazelle and Palios [5] decomposes any 3d polyhedron of zero genus with n vertices and r reflex edges (a measure of non-convexity) into $O(n + r^2)$ tetrahedra in $O((n + r^2) \log r)$ time. There are efficient algorithms as well as robust implementations to generate constrained Delaunay tetrahedralisation [17] of any 3d polyhedra are available [16, 19, 20, 18].

In this paper, we study the problem of tetrahedralising a Chazelle polyhedron without modifying its exterior boundary, which means, Steiner points are only placed in the interior of it. The remainder of this paper is organised as follows: In Section 2 we briefly review the construction of the Chazelle polyhedron, and discuss its basic properties. In Section 3 we perform a polyhedral reduction of the Chazelle polyhedron by removing polyhedra which are tetrahedralisable. This leads to a 3d indecomposable polyhedron, which will be defined as the reduced Chazelle polyhedron $\Phi_{N,\varepsilon}$ with the two parameters N and ε. We then study how to tetrahedralise the reduced Chazelle polyhedron by placing only interior Steiner points in Section 4. We first define a set of interior Steiner points in a reduced Chazelle polyhedron $\Phi_{N,\varepsilon}$, and then we prove that there exists a tetrahedralisation of $\Phi_{N,\varepsilon}$ with this set of Steiner points. There is a correspondence between a sequence of edge flips and a tetrahedralisation of a 3d polyhedron. This allow us to transform our 3d tetrahedralisation problem into a 2d triangulation transformation problem. A difficulty is due to the non-convexity of the reduced Chazelle polyhedron, we show that every edge flip generated by our transformation algorithm corresponds to a valid tetrahedron in $\Phi_{N,\varepsilon}$.

2 The Chazelle Polyhedron

The essential geometry of a Chazelle polyhedron is a saddle surface, which is a hyperbolic paraboloid, specified by the equation $z = x^2 - y^2$ or $z = xy$, see Figure 1 left. It is a doubly ruled surface which means that it can be made by two different sets of lines.

The Chazelle polyhedron is constructed by cutting notches from the two opposite faces of a cube, see Figure 1 Right. Placing the bottom face of the cube in the xy-plane and aligning its edges with the x- and y-axis. Call the notches on top and bottom of the cube *top notches* and *bottom notches*, respectively. Let all the bottom notches parallel to the y-axis and lie on the saddle surface $z = xy$, and let all the top notches parallel to the x-axis and lie on the saddle surface $z = xy + \varepsilon$, for a small positive constant $\varepsilon > 0$. In general, there may be an arbitrary number of notches. This leads to a family of such polyhedra which are parametrised by the number of notches N and the thickness ε.

Assume there are $N+1$ notches on each face of the cube, where $N \geq 1$. Label the vertices of the top and bottom notches as: a_i, b_i, α_i, and β_i, where $i = 0, \ldots, N$, respectively (see

Figure 1 Right). A choice of the coordinates of these vertices given by Chazelle is:

$$\begin{aligned} a_i &:= (-1, i, -i), \\ b_i &:= (N+1, i, i(N+1)), \\ \alpha_i &:= (i, -1, -i+\varepsilon), \\ \beta_i &:= (i, N+1, i(N+1)+\varepsilon), \end{aligned}$$

for integers $0 \leq i \leq N$. Therefore, the length of the top and bottom faces of the cube is $N+2$. The lower face of the cube lies below the plane $z = -N$, and the top face of the cube lies above the plane $z = N(N+1)+\varepsilon$.

Let $\Pi_{N,\varepsilon}$ be a Chazelle polyhedron with $N+1$ notches and a thickness ε. Let Σ be the region between the two hyperbolic paraboloids in $\Pi_{N,\varepsilon}$. If ε is sufficiently small, Σ has volume $\Theta(\varepsilon^2 N^2)$, and every convex polyhedron that lies in Σ necessarily has volume $o(\varepsilon^2)$ or smaller. These two facts are enough to show that Σ needs at least $\Omega(N^2)$ convex polyhedra to be decomposed. This also implies that it needs many Steiner points to be tetrahedralised.

Indeed the real problematic part in $\Pi_{N,\varepsilon}$ is the region Σ, which is the space formed between the two saddle surfaces. This region can be made arbitrarily small by letting $\varepsilon \to 0$, which can cause the failure of many existing tetrahedralisation algorithms. In the next section, we will study the geometric structure of Σ.

3 Reduced Chazelle Polyhedra

Let $\Pi_{N,\varepsilon}$ be the Chazelle polyhedron with $N+1$ notches and a thickness ε. In this section, we will reduce the volume of $\Pi_{N,\varepsilon}$ by removing the regions that are tetrahedralisable until it is not possible anymore. Our reduction is done in three steps. In each step, we will insert some interior edges into $\Pi_{N,\varepsilon}$. This allows us to remove some regions which are tetrahedralisable. These steps are described below (see also Figure 2):

Step (1). This step first inserts the four interior edges of $\Pi_{N,\varepsilon}$:

$$a_0\alpha_0, b_0\alpha_N, a_N\beta_0, \text{ and } b_N\beta_N.$$

It then removes the four (corner) tetrahedra: $t_0, \ldots, t_3$ from $\Pi_{N,\varepsilon}$.

Step (2). This step first inserts the following interior edges of $\Pi_{N,\varepsilon}$:

$$\begin{aligned} & \{\alpha_N b_i, a_0\alpha_i \mid i = 1, \ldots, N\}, \\ \cup\ & \{\beta_0 a_i, b_N\beta_i \mid i = 0, \ldots, N-1\}, \\ \cup\ & \{a_i a_{i+1}, b_i b_{i+1}, \alpha_i\alpha_{i+1}, \beta_i\beta_{i+1} \mid i = 0, \ldots, N-1\}. \end{aligned}$$

It then removes the four corner polyhedra: A, B, C, and D from $\Pi_{N,\varepsilon}$.

Step (3). This step first inserts the following interior edges of $\Pi_{N,\varepsilon}$:

$$\begin{aligned} & \{\alpha_i\beta_j \mid i = 0, \ldots, N-1 \text{ and } j = 1, \ldots, N\} \\ \cup\ & \{a_i b_j \mid i = 1, \ldots, N \text{ and } j = 0, \ldots, N-1\} \end{aligned}$$

Then it removes the $2N$ polyhedra: $E_1, \ldots, E_N$ and $F_1, \ldots, F_N$ of $\Pi_{N,\varepsilon}$.

At the end of this reduction process, we obtain a polyhedron $\Phi_{N,\varepsilon} \subset \Pi_{N,\varepsilon}$, where

$$\Phi_{N,\varepsilon} := \Pi_{N,\varepsilon} - (t_0 + \ldots, t_3) - (A + B + C + D) - (E_1 + \ldots + E_N) - (F_1 + \ldots + F_N).$$

The vertices of $\Phi_{N,\varepsilon}$ are endpoints of the two sets of lines on the two saddle surfaces $z = xy$ and $z = xy + \varepsilon$. We will call $\Phi_{N,\varepsilon}$ a *reduced Chazelle polyhedron.*

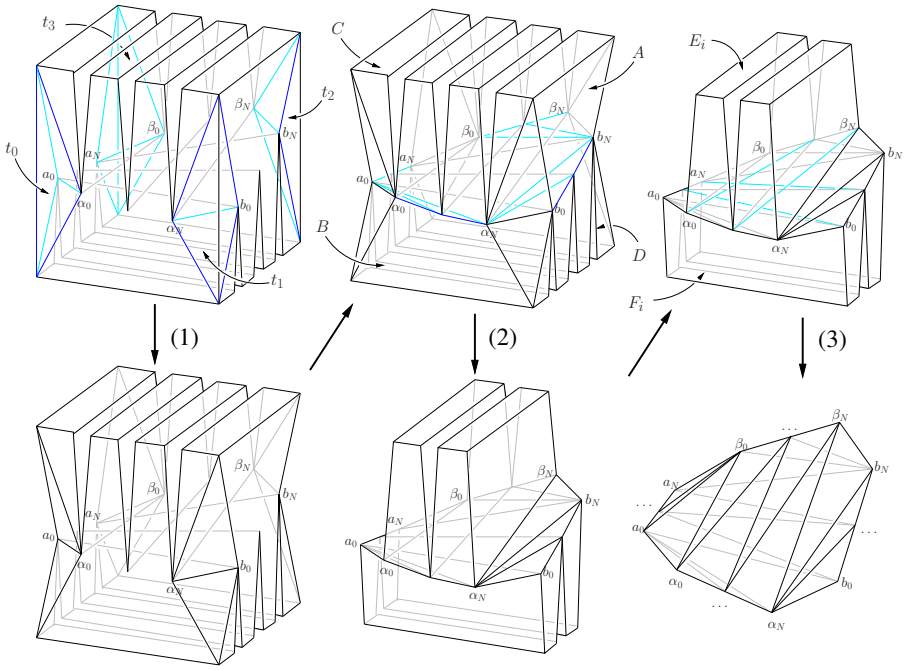

Figure 2 The volume reduction process. The three steps of the reduction are shown by the arrows. It starts from the Chazelle polyhedron (top-left) and ends at the reduced Chazelle polyhedron (bottom-right). At each step, a set of interior edges (shown in blue) is first inserted, and then a number of tetrahedra $t_1, \ldots, t_4$, and polyhedra: A, B, C, D, $E_1, \ldots, E_N$, and $F_1, \ldots, F_N$ are removed.

It can be shown that all the regions that have been removed from the original Chazelle polyhedron, i.e., $t_0, \ldots, t_3$, A, B, C, D, $E_1, \ldots, E_N$ and $F_1, \ldots, F_N$ are all tetrahedralisable with a linear number of tetrahedra (see Appendix). Therefore the reason that causes the Chazelle polyhedron to be indecomposable is due to the reduced Chazelle polyhedron.

Alternatively, we can define a *reduced Chazelle polyhedron* $\Phi_{N,\varepsilon}$ as follows: The set of vertices of $\Phi_{N,\varepsilon}$ are

$$\{a_i, b_i, \alpha_i, \beta_i \,|\, i = 0, \ldots, N\},$$

where

$$a_i := (-1, i, -i), \text{ and } b_i := (N+1, i, i(N+1)),$$

are endpoints of the line segments on the saddle surface $z = xy$, and

$$\alpha_i := (i, -1, -i + \varepsilon), \text{ and } \beta_i := (i, N+1, i(N+1) + \varepsilon),$$

are endpoints of the line segments on $z = xy + \varepsilon$.

The set of boundary faces of $\Phi_{N,\varepsilon}$ are:

(1) $\{\alpha_i\beta_j\beta_{j-1}, \alpha_i\beta_j\alpha_{i+1} \,|\, i = 0, \ldots, N-1, \text{ and } j = 1, \ldots, N\}$;
(2) $\{\alpha_N b_i b_{i+1}, \beta_0 a_i a_{i+1} \,|\, i = 0, \ldots, N-1\}$;
(3) $\{a_i b_j a_{i-1}, a_i b_j b_{j+1} \,|\, i = 1, \ldots, N, \text{ and } j = 0, \ldots, N-1\}$;
(4) $\{a_0\alpha_i\alpha_{i+1}, b_N\beta_i\beta_{i+1} \,|\, i = 0, \ldots, N-1\}$.

The triangles in (1) and (2) are called *top triangles* of $\Phi_{N,\varepsilon}$, and the triangles in (3) and (4) are called *bottom triangles* of $\Phi_{N,\varepsilon}$, as they are viewed from the top of the xy-plane, see

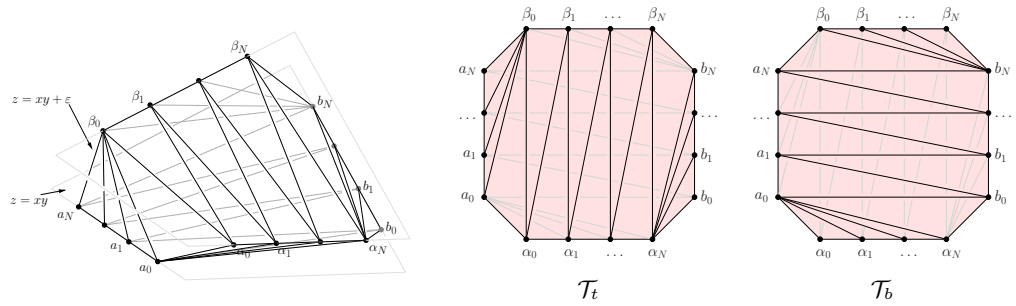

Figure 3 Left: A reduced Chazelle polyhedron $\Phi_{3,\varepsilon}$. Right: The top triangulation $\mathcal{T}_t$ includes the set of top faces as viewed from the point $(0, 0, +\infty)$ toward the $-z$ direction. The bottom triangulation $\mathcal{T}_b$ includes the set of bottom faces viewed from the point $(0, 0, -\infty)$ toward the $+z$ direction.

Figure 3. In particular, the top triangles and bottom triangles form two triangulations of a convex polygon, they are called the *top triangulation* $\mathcal{T}_t$ and the *bottom triangulation* $\mathcal{T}_b$ of $\Phi_{N,\varepsilon}$, respectively. The parameter ε is called the *thickness* of $\Phi_{N,\varepsilon}$.

4 Tetrahedralisations of Reduced Chazelle Polyhedra

In this section, we consider our main question: to tetrahedralise a reduced Chazelle polyhedron $\Phi_{N,\varepsilon}$ without modifying its exterior boundary. For this purpose, Steiner points can be only added in the interior of $\Phi_{N,\varepsilon}$. We will propose a set of interior Steiner points in $\Phi_{N,\varepsilon}$ and show there exists a tetrahedralisation of $\Phi_{N,\varepsilon}$ with this set of Steiner points. Before we do that, we will review a nice relation between a sequence of edge flips and a tetrahedralisation of a 3d polyhedron. This allows us to transform our tetrahedralisation problem by a 2d triangulation transformation problem.

4.1 Edge Flips and Tetrahedralisations

If we ignore the z-coordinates of the vertices of $\Phi_{N,\varepsilon}$, the top and bottom faces of $\Phi_{N,\varepsilon}$ give two different triangulations of a two-dimensional convex polygon Q whose vertices are vertices of $\Phi_{N,\varepsilon}$ projecting onto the xy-plane, see Figure 3. It is well known that there exists a sequence of edge flips that will transform one triangulation to another one of Q.

Sleator et al [21] showed the correspondence between a sequence of edge flips and a tetrahedralisation of a 3d convex polyhedron. The basic idea is to view every edge flip as removing a tetrahedron from the polyhedron. By fixing a position of a 3d convex polyhedron P, the orthogonal projection of P (i.e., ignoring the z-coordinates of points in P) is a convex polygon Q in the xy-plane. At this moment, one only "sees" the outer boundary faces of P which is a 2d triangulation $\mathcal{T}_1$ of Q. Now an edge flip in $\mathcal{T}_1$ corresponds the removal of a tetrahedron from P such that the two lower faces of this tetrahedron are replaced by the two upper faces of it. After a sequence of such edge flips, the hidden boundary faces of P, which is another triangulation $\mathcal{T}_2$ of Q, appears. As a consequence, the collection of removed tetrahedra and their faces gives a tetrahedralisation of P. Moreover, the length of the flip sequence is equal to the total number of tetrahedra in this tetrahedralisation. The example of Sleator et al [21] is reproduced (correctly) in Figure 4.

However, not every tetrahedralisation of a 3d polyhedron is associated to a sequence of flips. This is even true for convex polyhedron, as shown in Sleator et al [21]. A reduced

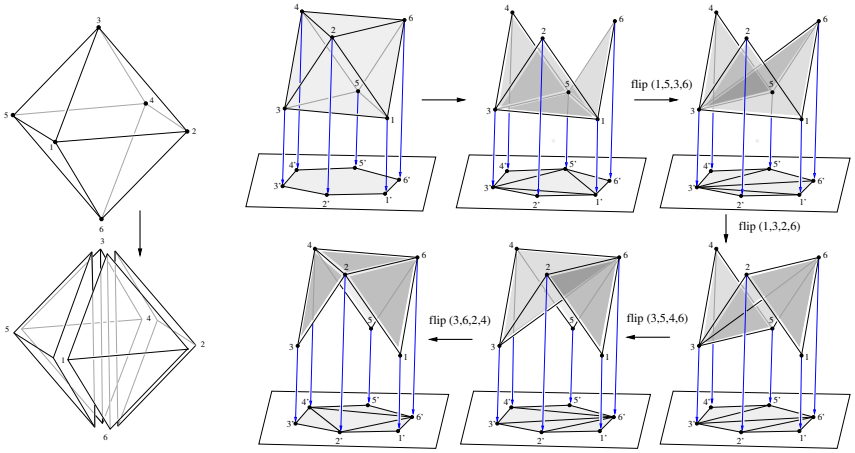

Figure 4 Letf: A tetrahedralisation of an octahedron with four tetrahedra. Right: A sequence of edge flips which corresponds to the tetrahedralisation on the left.

Chazelle polyhedron $\Phi_{N,\varepsilon}$ is non-convex. The main problem caused by the non-convexity is that a flippable edge in the plane may not correspond to a valid tetrahedron in the interior of a non-convex polyhedron. Indeed, it is possible that none of the flippable edge in the top and bottom triangulation of $\Phi_{N,\varepsilon}$ will create a valid tetrahedron in the interior of $\Phi_{N,\varepsilon}$. This problem can only be resolved if there are Steiner points in $\Phi_{N,\varepsilon}$.

4.2 A Placement of Interior Steiner Points

Recall that the volume of a Chazelle polyhedron $\Phi_{N,\varepsilon}$ is sandwiched by two saddle surfaces with a thickness ε. We will place a set of $(N+1)^2$ interior Steiner points,

$$\mathcal{S} := \{s_{i,j} \mid i,j = 0,\ldots,N\},$$

where

$$s_{i,j} := (i, j, ij + \omega), \text{ and } 0 < \omega < \varepsilon,$$

into the interior of $\Phi_{N,\varepsilon}$. These Steiner points are directly at the intersections of the two set of lines in the xy-plane and all lie on the saddle surface $z = xy + \omega$, where $0 < \omega < \varepsilon$, see Figure 5. We will show that there exist a tetrahedralization of a reduced Chazelle polyhedron $\Phi_{N,\varepsilon}$ with this set of Steiner points.

Due to the correspondence of edges flips and tetrahedralisations, we will tackle our tetrahedralisation problem by using two-dimensional triangulations. In particular, we will first show a transformation between the two triangulations $\mathcal{T}_t$ and $\mathcal{T}_b$ (shown in Figure 3), which includes the set $\mathcal{S}$ of Steiner points. And then show this transformation indeed corresponds to a tetrahedralisation of $\Phi_{N,\varepsilon}$.

4.3 The Transformation Algorithm

For simplifying the transformation algorithm as well as our proof, it is more convenient to work on a modified polyhedron, denoted as $\Phi^s_{N,\varepsilon}$. It is only different to $\Phi_{N,\varepsilon}$ at the four corners. The modifications are summarised in the following.

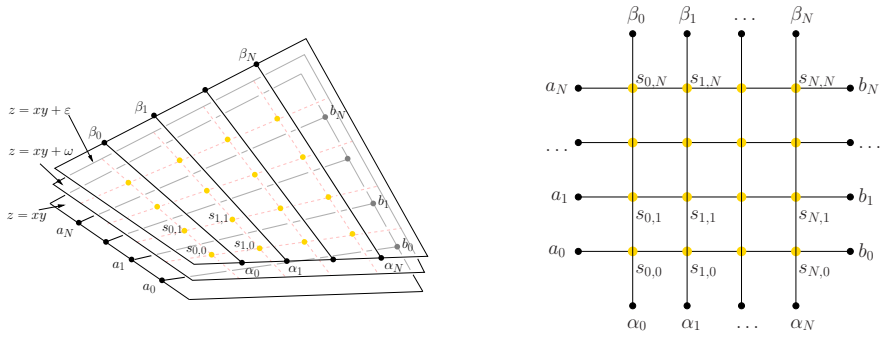

Figure 5 The interior Steiner points, $\{s_{i,j} \mid i,j = 0,\ldots,N\}$, are placed directly at the intersections of the two set of lines in the xy-plane and all lie on the saddle surface $z = xy + \omega$, where $0 < \omega < \varepsilon$.

- Introduce four new Steiner points on the saddle surface $z = xy + \omega$, they are located on the corners of $\Phi_{N,\varepsilon}$, i.e., let

$$\mathcal{S}^s := \mathcal{S} \cup \{s_{-1,-1}, s_{-1,N+1}, s_{N+1,-1}, s_{N+1,N+1}\},$$

  where

$$\begin{aligned} s_{-1,-1} &:= (-1,-1,1+\omega), \\ s_{-1,N+1} &:= (-1,N+1,-(N+1)+\omega), \\ s_{N+1,-1} &:= (N+1,-1,-(N+1)+\omega), \\ s_{N+1,N+1} &:= (N+1,N+1,(N+1)^2+\omega). \end{aligned}$$

- Relabelling the vertices of $\mathcal{T}_t$ and $\mathcal{T}_b$ as following:

$$\begin{array}{llllll} a_0 & \to & s_{-1,0}, & \ldots, & a_N & \to & s_{-1,N} \\ b_0 & \to & s_{N+1,0}, & \ldots, & b_N & \to & s_{N+1,N} \\ \alpha_0 & \to & s_{0,-1}, & \ldots, & \alpha_N & \to & s_{N,-1} \\ \beta_0 & \to & s_{0,N+1}, & \ldots, & \beta_N & \to & s_{N,N+1} \end{array}$$

- Modify $\mathcal{T}_t$ and $\mathcal{T}_b$ to include the new Steiner points, i.e., let

$$\begin{aligned} \mathcal{T}_t^s := \; & \mathcal{T}_t \setminus \{s_{-1,0}s_{0,-1}s_{0,N+1}, s_{N,-1}s_{N,N+1}s_{N+1,N}\} \\ \cup \; & \{s_{-1,-1}s_{0,N+1}s_{-1,0}, s_{-1,-1}s_{0,N+1}s_{0,-1}, s_{-1,N}s_{0,N+1}s_{-1,N+1}\} \\ \cup \; & \{s_{N,-1}s_{N+1,N+1}s_{N,N+1}, s_{N,-1}s_{N+1,N+1}s_{N+1,N}, s_{N,-1}s_{N+1,-1}s_{N+1,0}\}, \end{aligned}$$

  and

$$\begin{aligned} \mathcal{T}_b^s := \; & \mathcal{T}_b \setminus \{s_{-1,0}s_{N+1,0}s_{N,-1}, s_{N+1,N}s_{-1,N}s_{-1,N+1}\} \\ \cup \; & \{s_{-1,0}s_{N+1,-1}s_{N,-1}, s_{-1,0}s_{N+1,-1}s_{N+1,0}, s_{-1,-1}s_{-1,0}s_{0,-1}\} \\ \cup \; & \{s_{N,-1}s_{N+1,N+1}s_{N,N+1}, s_{N,-1}s_{N+1,N+1}s_{N+1,N}, s_{N,-1}s_{N+1,-1}s_{N+1,0}\}. \end{aligned}$$

Figure 6 illustrates an example after making these modifications on the example in Figure 3. The volume of the original reduced Chazelle polyhedron $\Phi_{N,\varepsilon}$ is completely included in the modified reduced Chazelle polyhedron $\Phi^s_{N,\varepsilon}$. Although the transformation algorithm described below will only apply to the modified reduced Chazelle polyhedron $\Phi^s_{N,\varepsilon}$, this technique also applies to tetrahedralise the reduced Chazelle polyhedron $\Phi_{N,\varepsilon}$ as well.

From now on, we will focus on the tetrahedralisation of the modified reduced Chazelle polyhedron $\Phi^s_{N,\varepsilon}$ with the set $\mathcal{S}$ of interior Steiner points.

Our algorithm will use two basic local transformation operations: `split_edge` and `flip_edge`, which are defined below.

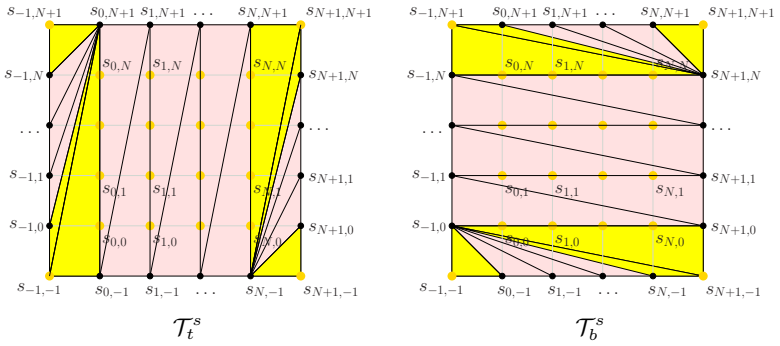

Figure 6 The modified top and bottom triangulations of $\Phi^s_{N,\varepsilon}$. There are four new vertices: $s_{-1,-1}$, $s_{N+1,-1}$, $s_{-1,N+1}$, and $s_{N+1,N+1}$. The newly added triangles are shown in yellow.

- The `split_edge`(a, b, p) operation takes an edge ab and a point p that lies in the interior of ab as inputs. It replaces the two triangles abc and bad sharing at the edge ab by four triangles apc, bpc, apd, and bpd.
- The `flip_edge`(a, b, c, d) operation takes two triangles abc and bad sharing at the edge ab, and replaces them by another two triangles cda, and cdb sharing at the edge cd.

INPUT: $\mathcal{T}_t^s$

```
1   // inserting Steiner points
2   for I = 0 to N do
3     for J = 0 to N do
4       split_edge(s_{I,J-1}, s_{I,N+1}, s_{I,J});
5     endfor
6   endfor
7   // flipping edges
8   for I = 0 to ⌊(N+2)/2⌋ do
9     // flipping upper edges
10    for J = 0 to N + 1 do
11      for K = I to N − I do
12        edge_flip(s_{J+1,N+1−I}, s_{J,K−1},
              s_{J+1,N−I}, s_{J,K});
13      endfor
14    endfor
15    // flipping lower edges
16    for J = 0 to N + 1 do
17      for K = I + 1 to N − I do
18        edge_flip(s_{J,I−1}, s_{J+1,N+1−K},
              s_{J,I}, s_{J+1,N−K});
19      endfor
20    endfor
21  endfor
22  return T_t^m;
```

INPUT: $\mathcal{T}_b^s$

```
1   // inserting Steiner points
2   for I = 0 to N do
3     for J = 0 to N do
4       split_edge(s_{I−1,J}, s_{N+1,J}, s_{I,J});
5     endfor
6   endfor
7   // flipping edges
8   for I = 0 to ⌊(N+2)/2⌋ do
9     // flipping left edges
10    for J = 0 to N + 1 do
11      for K = I to N − I do
12        edge_flip(s_{I−1,J}, s_{N+1−K,J−1},
              s_{I,J}, s_{N−K,J−1});
13      endfor
14    endfor
15    // flipping right edges
16    for J = 0 to N + 1 do
17      for K = I + 1 to N − I do
18        edge_flip(s_{N+1−I,J−1}, s_{K−1,J},
              s_{N−I,J−1}, s_{K,J});
19      endfor
20    endfor
21  endfor
22  return T_b^m;
```

Figure 7 The transformation algorithm. It is divided into two parts, where one works in the top triangulation $\mathcal{T}_t^s$, and the other works in the bottom triangulation $\mathcal{T}_b^s$.

Our algorithm is given in Figure 7. This algorithm transforms the two triangulations, $\mathcal{T}_t^s$ and $\mathcal{T}_b^s$, simultaneously. It works in two steps. In the first step, it uses `split_edge` operations to insert the interior Steiner points into both $\mathcal{T}_t^s$ and $\mathcal{T}_b^s$. In the second step, it uses `edge_flip` operations to transform $\mathcal{T}_t^s$ and $\mathcal{T}_b^s$ into two *middle triangulations*, $\mathcal{T}_t^m$ and $\mathcal{T}_b^m$, respectively. An example of this algorithm is shown in Figure 8 and 9.

Note that the two resulting triangulations $\mathcal{T}_t^m$ and $\mathcal{T}_b^m$ only different by $(N+1)^2$ diagonal flips. Hence this algorithm will successfully transform $\mathcal{T}_t^s$ to $\mathcal{T}_b^s$ or vice versa.

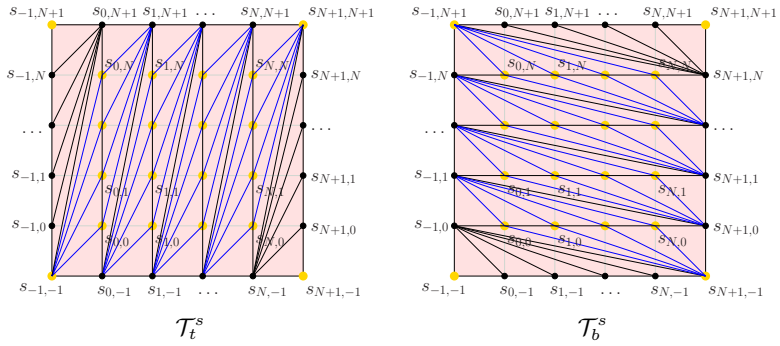

Figure 8 An example result of the first step of the transformation algorithm. All Steiner points are inserted by splitting the edges.

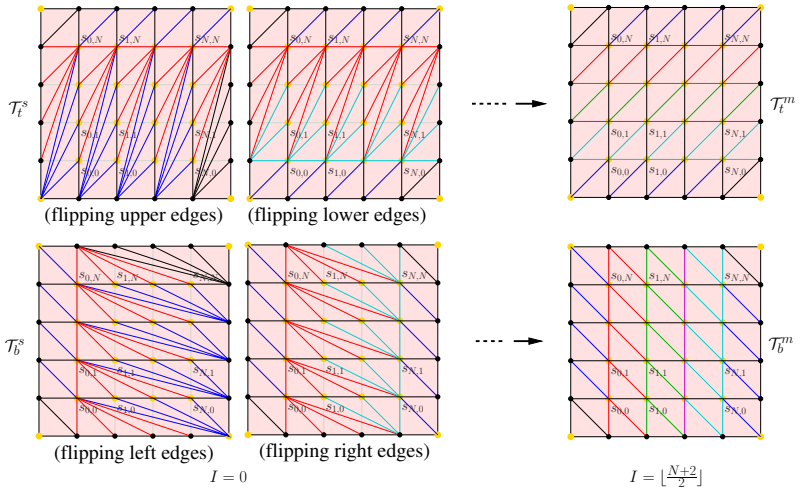

Figure 9 An example result of the second step of the transformation algorithm. Two sequences of edge flips are applied on top and bottom triangulations, respectively. The resulting two triangulations $\mathcal{T}_t^m$ and $\mathcal{T}_b^m$ are shown on the right.

4.4 Proof of Correctness

In this section, we will show that the transformation algorithm does give a tetrahedralisation of the modified reduced Chazelle polyhedron $\Phi^s_{N,\varepsilon}$.

Consider the case when two planar triangles abc and abd are split by a point p that lies in the interior of the edge ab. It results four triangles, apc, bpc, apd, and bpd. Now placing the two original triangles abc and bad in $\mathbb{R}^3$, and shift the point p slightly away from the edge ab, and let the projection of them in the plane still remains the same picture. What we have in $\mathbb{R}^3$ are two tetrahedra $abpc$ and $abpd$. If we look from the top of them we see the two faces: abc and abd, and from bottom we see the other four faces all containing p. Hence a `split_edge` operation interchanges the two sets of outer faces of these two tetrahedra.

The `split_edge` operations in our algorithm (in the lines from 2 to 6) correspond to the removals of tetrahedra from $\Phi^s_{N,\varepsilon}$, and at the same time, the insertions of the Steiner points. This algorithm starts from the most outer boundary faces of $\Phi^s_{N,\varepsilon}$, for an example, the two faces $s_{J,-1}s_{J,N+1}s_{J-1,-1}$ and $s_{J,-1}s_{J,N+1}s_{J+1,N+1}$ sharing at the boundary edge $s_{J,-1}s_{J,N+1}$,

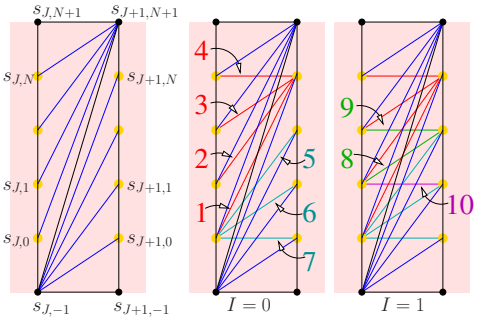

Figure 10 An example of the sequence of edge flips applied on one section of the top triangulations $\mathcal{T}_t^s$. Left is the initial triangulation before the edge flips. Right shows the sequence is the newly created edges with their indices by the flip sequence.

and removes two tetrahedra $s_{J,-1}s_{J,N+1}s_{J-1,-1}s_{J,0}$ and $s_{J,-1}s_{J,N+1}s_{J+1,N+1}s_{J,0}$ from $\Phi^s_{N,\varepsilon}$. The removal of these two tetrahedra makes a "dent" in the outer boundary of $\Phi^s_{N,\varepsilon}$ which has now the four new triangles (the lower faces of the two removed tetrahedra) with the interior Steiner point $s_{J,0}$ on its boundary. The next `split_edge` operation continues to remove tetrahedra from the just exposed new boundary faces. For the same example as above, the two faces $s_{J,0}s_{J,N+1}s_{J-1,-1}$ and $s_{J,0}s_{J,N+1}s_{J+1,N+1}$ sharing at the boundary edge $s_{J,0}s_{J,N+1}$ are split, and the new interior Steiner points $s_{J,1}$ is inserted on the boundary. This process ends after all interior Steiner points are on the boundary $\Phi^s_{N,\varepsilon}$, as viewed in Figure 8. Note that the tetrahedra removed from top and bottom triangulations will not overlap, since they are separated by the saddle surface $z = xy + \omega$.

Now we turn to the second step of our algorithm, which uses the `flip_edge` operations to transform the top and bottom triangulations. We already showed that each `flip_edge` operation corresponds to a tetrahedron. We still need to show that this tetrahedron is valid, i.e., the removal of it does decrease the volume of $\Phi^s_{N,\varepsilon}$.

In $\mathcal{T}_t^b$, all edges between the two line segments $s_{J,-1}s_{J,N+1}$ and $s_{J+1,-1}s_{J+1,N+1}$ are divided into two groups by the diagonal line segment $s_{J,-1}s_{J+1,N+1}$, where $J = -1, \ldots, N$. They are called *upper* and *lower* edges, respectively, see an example in Figure 10. Similarly, all edges in $\mathcal{T}_b^s$ between the two line segments $s_{-1,J}s_{N+1,J}$ and $s_{-1,J+1}s_{N+1,J+1}$ are divided into two groups by the diagonal line segment $s_{-1,J}s_{N+1,J-1}$, where $J = -1, \ldots, N$. They are called *left* and *right* edges, respectively.

Our transform algorithm will automatically generate two sequences of edge flips, i.e., the pseudocode from lines 8 to 21 in Figure 7, one in the top $\mathcal{T}_t^s$ and one in the bottom $\mathcal{T}_b^s$ triangulations. Each flip sequence is also divided into two subsequences, which are the flips to create the upper and lower edges in $\mathcal{T}_t^s$ and the flips to create left and right edges in $\mathcal{T}_b^s$. The order of these flip sequences ensures that the edges needed for the next flip exist. Figure 10 gives an example of all edges generated between one pair of line segments and the order of the edge flip sequence.

Now it remains to show that every edge flip in our algorithm will create a valid tetrahedron for $\Phi^s_{N,\varepsilon}$. In particular, there are four `flip_edge` operations (in line 12 and line 18 in Figure 7) in our algorithm, see Figure 11. They are used in the four subsequences of edge flips, respectively. Since each edge flip operation is a local operation, it is sufficient to show that each edge flip will create an interior edge of $\Phi^s_{N,\varepsilon}$. Hence the newly created edge together with the old edge form an interior tetrahedron of $\Phi^s_{N,\varepsilon}$. For this purpose, the following lemma

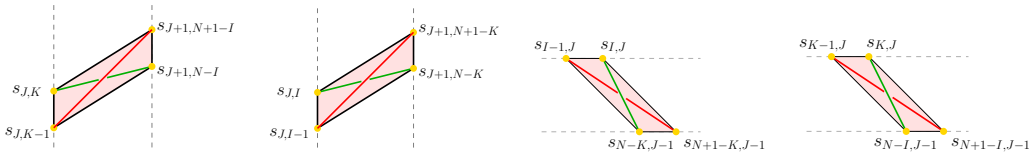

(1) in $\mathcal{T}_t^s$ upper (2) in $\mathcal{T}_t^s$ lower (3) in $\mathcal{T}_b^s$ left (4) in $\mathcal{T}_b^s$ right

Figure 11 The four types of edge flips in the algorithm. In these figures, red edges are the input edges, green edges are the resulting edges. Each pair of red and green edges forms a tetrahedron in the interior of $\Phi^s_{N,\varepsilon}$.

is needed.

▶ **Lemma 1.** *Let $det(s_1, s_2, s_3, s_4)$ denote the determinant of the four points $s_1, \ldots, s_4 \in \mathbb{R}^3$. Then the following determinants on the set of Steiner points are all constant.*

$$det(s_{J+1,N+1-I}, s_{J,K-1}, s_{J+1,N-I}, s_{J,K}) \equiv 1 \tag{1}$$
$$det(s_{J,I-1}, s_{J+1,N+1-K}, s_{J,I}, s_{J+1,N-K}) \equiv 1 \tag{2}$$
$$det(s_{I-1,J}, s_{N+1-K,J-1}, s_{I,J}, s_{N-K,J-1}) \equiv -1 \tag{3}$$
$$det(s_{N+1-I,J-1}, s_{K-1,J}, s_{N-I,J-1}, s_{K,J}) \equiv -1 \tag{4}$$

The above equalities can be proven by direct calculations (given in Appendix).

This lemma ensures that each `flip_edge` operation in our algorithm will indeed create a valid tetrahedron in $\Phi^s_{N,\epsilon}$. In particular, equation (1) indicates that the

$$\texttt{flip\_edge}(s_{J+1,N+1-I}, s_{J,K-1}, s_{J+1,N-I}, s_{J,K})$$

operation in the top triangulation $\mathcal{T}_t^s$ will create a new edge $s_{J+1,N-I}s_{J,K}$ that lies below the old edge $s_{J+1,N+1-I}s_{J,K-1}$, see Figure 11 (1). And the equation (3) indicates that the

$$\texttt{flip\_edge}(s_{I-1,J}, s_{N+1-K,J-1}, s_{I,J}, s_{N-K,J-1})$$

operation in the bottom triangulation $\mathcal{T}_b^s$ will create a new edge $s_{I,J}s_{N-K,J-1}$ that lies above the old edge $s_{I-1,J}s_{N+1-K,J-1}$, see Figure 11 (3). The same are true for the other two `flip_edge` operations.

By this lemma, all tetrahedra correspond to our edge flip sequences are valid. Another surprising fact is that the volumes of these tetrahedra are all equal and are independent of the parameters N, ε, and ω.

We thus can prove the following theorem:

▶ **Theorem 2.** *There exists a tetrahedralisation of $\Phi^s_{N,\varepsilon}$ with the set $\mathcal{S}$ of interior Steiner points.*

Proof. Given a $\Phi^s_{N,\varepsilon}$, we apply the transformation algorithm in Figure 7 from its top and bottom triangulations to reduce the volume of $\Phi^s_{N,\varepsilon}$ by removing tetrahedra from $\Phi^s_{N,\varepsilon}$ corresponding to the `split_edge` and `flip_edge` operations. This will reduce $\Phi^s_{N,\varepsilon}$ into a 3d polyhedron P which has the two triangulations $\mathcal{T}_t^m$ and $\mathcal{T}_b^m$ (shown in Figure 9 right) as its boundary. It is easy to see that the set of tetrahedra

$$\mathcal{T}_m := \{s_{I-1,J-1}s_{I,J-1}s_{I-1,J}, s_{I,J} \mid I, J = 1, \ldots, N+1\}.$$

tetrahedralises P. ◀

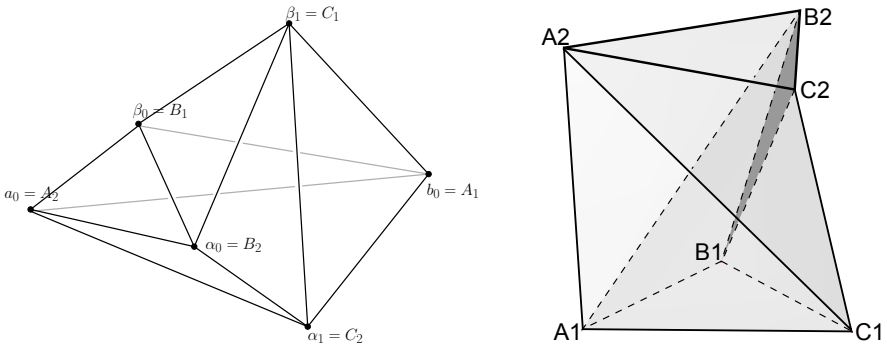

Figure 12 The generalised Chazelle polyhedron $\Pi_{0,1,\varepsilon}$ (left) has the same combinatorial structure as the Schönhardt polyhedron (right). The map between the vertices of them is given.

5 Generalised Chazelle Polyhedra

In the Paper "On Indecomposable Polyhedra" by F. Bagemihl [1] he proves the following

▶ **Theorem 3** ([1]). *If n is an integer not less than 6, then there exists a polyhedron, π_n, with n vertices and the following properties:*

(I) *π_n is simple and every one of its faces is a triangle.*

(II) *If τ is a tetrahedron, each of whose vertices is a vertex of π_n, then not every interior point of τ is an interior point of π_n.*

(III) *Every open segment whose endpoints are vertices of π_n, but which is not an edge of π_n, lies wholly exterior to π_n.*

Bagemihl's Theorem claims there exists a family of such indecomposable polyhedra. He also provides a construction of a class of polyhedra based on the Schönhardt polyhedron [15], which are called *Bagemihl polyhedra*[1], that belong to this family. In [10] we generalised Bagemihl polyhedra to construct a larger family of 3d indecomposable polyhedra that also belong to this family. In this section, we show a new class of 3d indecomposable in this family by generalising the reduced Chazelle polyhedra.

The polyhedron we want to construct uses the same two saddle surfaces with a sufficiently small thickness ε. Now the numbers of two sets of line segments are not necessarily the same. Hence we use two parameters, N_t and N_b, which count the numbers of top and bottom line segments, respectively. We call such a polyhedron a *generalised Chazelle polyhedron*, denoted as $\Pi_{N_b,N_t,\varepsilon}$. We provide the formal definition of $\Pi_{N_b,N_t,\varepsilon}$ in appendix.

The class of generalised Chazelle polyhedra has in general a different combinatorial structure than the Bagemihl polyhedra and our generalised class of polyhedra. Interestingly, the simplest one, i.e., $\Pi_{0,1,\varepsilon}$, has the same combinatorial structure of the Schönhardt polyhedron [15]. It is illustrated in Figure 12.

It is obvious, one needs interior Steiner points to tetrahedralise a generalised Chazelle polyhedron $\Pi_{N_b,N_t,\varepsilon}$. The lower bound of the number of Steiner points is $\Omega(N_bN_t)$. Our placement of Steiner points and our algorithm given in this paper are also applied to tetrahedralise any generalised Chazelle polyhedron.

6 Discussions

In this paper, we studied the problem of tetrahedralising reduced Chazelle polyhedra with interior Steiner points. We proposed a placement of Steiner points and show the existence of

a tetrahedralisation with these Steiner points. In practice, the questions like “where to place Steiner points" and “How many of them are necessary?" are very important to know in order to design correct and efficient algorithms. Our result gives at least some suggestion on where the Steiner points could be placed. However, the optimal number of Steiner points remains an open question.

The set $\mathcal{S}$ of interior Steiner points is independent of the thickness ε of $\Phi^s_{N,\varepsilon}$. Here the thickness ε plays an important role in the needed number of interior Steiner points.

- There are $(N+1)^2$ Steiner points in $\mathcal{S}$ and it is indeed necessary to have all of them when the thickness ε is sufficiently small.
- If the thickness ε becomes larger, it is not necessary to use the full set of $(N+1)^2$ Steiner points. In particular, there must exists a bound on ε such that the reduced Chazelle polyhedron $\Phi^s_{N,\varepsilon}$ needs only a linear number of Steiner points.
- If the ε is larger enough, the reduced Chazelle polyhedron becomes directly tetrahedralisable, i.e., no Steiner point is needed. There must exist such a bound on ε.

It is an interesting question to find the relation of ε and the number of Steiner points. This may be a interesting theoretical question for our future work.

Finally, there are indeed many possibilities to generalise the Chazelle polyhedron. One of such examples is found in [7]. More generally, it is possible to use any doubly-ruled surfaces instead of the saddle surfaces as the basic geometry structure.

References

1 F. Bagemihl. On indecomposable polyhedra. *The American Mathematical Monthly*, 55(7):411–413, 1948.

2 M. Bern. Compatible tetrahedralizations. In *Proc. 9th Annual ACM Symposium on Computational Geometry*, pages 281–288, 1993.

3 Marshall W. Bern and David Eppstein. Mesh generation and optimal triangulation. In Ding-Zhu Du and Frank Kwang-Ming Hwang, editors, *Computing in Euclidean Geometry*, number 4 in Lecture Notes Series on Computing, pages 47–123. World Scientific, second edition, 1995.

4 Bernard Chazelle. Convex partition of polyhedra: a lower bound and worst-case optimal algorithm. *SIAM Journal on Computing*, 13(3):488–507, 1984.

5 Bernard Chazelle and Leonidas Palios. Triangulating a non-convex polytope. *Discrete & Computational Geometry*, 5(3):505–526, 1990.

6 Mark de Berg and Chris Gray. Decompositions and boundary coverings of non-convex fat polyhedra. *Computational Geometry*, 43(2):73 – 83, 2010. Special Issue on the 24th European Workshop on Computational Geometry (EuroCG'08).

7 Jeff Erickson. Local polyhedra and geometric graphs. *Computational Geometry*, 31(1-2):101–125, 2005. Special Issue on the 19th Annual Symposium on Computational Geometry - SoCG 2003 19th Annual Symposium on Computational Geometry - SoCG 2003.

8 Paul-Louis George, Houman Borouchaki, and Eric Saltel. “Ultimate” robustness in meshing an arbitrary polyhedron. *International Journal for Numerical Methods in Engineering*, 58:1061–1089, 2003.

9 Paul-Louis George, Frédéric Hecht, and Eric Saltel. Automatic mesh generator with specified boundary. *Computer Methods in Applied Mechanics and Engineering*, 92:269–288, 1991.

10 Nadja Goerigk and Hang Si. On indecomposable polyhedra and the number of interior steiner points. WIAS Preprint No. 2142, June 2015.

11 J. Goodman and J. Pach. Cell decomposition of polytopes by bending. *Israel J. Mathematics*, 64:129–138, 1988.

12 Michael S. Paterson and F. Frances Yao. Efficient binary space partitions for hidden-surface removal and solid modeling. *Discrete & Computational Geometry*, 5(1):485–503, 1990.

13 Jörg Rambau. On a generalization of Schönhardt's polyhedron. In J. E. Goodman, J. Pach, and E. Welzl, editors, *Combinatorial and Computational Geometry*, volume 52, pages 501–516. MSRI publications, 2005.

14 Jim Ruppert and Raimund Seidel. On the difficulty of triangulating three-dimensional nonconvex polyhedra. *Discrete & Computational Geometry*, 7:227–253, 1992.

15 E. Schönhardt. Über die Zerlegung von Dreieckspolyedern in Tetraeder. *Mathematische Annalen*, 98:309–312, 1928.

16 Jonathan R. Shewchuk. Constrained Delaunay tetrahedralizations and provably good boundary recovery. In *Proc. 11th International Meshing Roundtable*, pages 193–204. Sandia National Laboratories, 2002.

17 Jonathan R. Shewchuk. General-dimensional constrained Delaunay and constrained regular triangulations, I: combinatorial properties. *Discrete & Computational Geometry*, 39:580–637, 2008.

18 Hang Si. TetGen, a Delaunay-based quality tetrahedral mesh generator. *ACM Trans. Math. Softw.*, 41(2):11:1–11:36, February 2015.

19 Hang Si and Klaus Gärtner. 3D boundary recovery by constrained Delaunay tetrahedralization. *International Journal for Numerical Methods in Engineering*, 85:1341–1364, 2011.

20 Hang Si and Jonathan R. Shewchuk. Incrementally constructing and updating constrained Delaunay tetrahedralizations with finite precision coordinates. In *Proceedings of the 21th International Meshing Rountable*, pages 173–190. Sandia National Laboratories, 2012.

21 Daniel D. Sleator, William P. Thurston, and Robert Endre Tarjan. Rotation distance,triangulations,and hyperbolic geometry. *J. Amer. Math. Soc.*, 1:647–682, 1988.

22 G. T. Toussaint, C. Verbrugge, C. Wang, and B. Zhu. Tetrahedralization of simple and non-simple polyhedra. In *Proc. 5th Canadian Conference on Computational Geometry*, pages 24–29, 1993.

23 Nigel P. Weatherill and Oubay Hassan. Efficient three-dimensional Delaunay triangulation with automatic point creation and imposed boundary constraints. *International Journal for Numerical Methods in Engineering*, 37:2005–2039, 1994.

A A Tetrahedral reduction of the Chazelle Polyhedron

We begin with the tetrahedralisation of the outer part of the polyhedron. We can describe it by giving the set of tetrahedra explicitly, so for the first we describe the used labels. An overview of the labels is given in Figure 13.

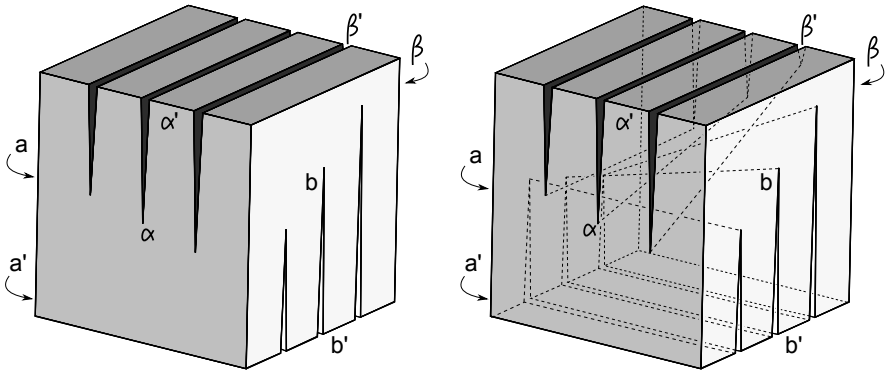

Figure 13 Left: the Chazelle polyhedron without showing interior edges, Right: interior edges are included. The labeling is sketched without giving the precise numbering. One can find them in the figures below. In this picture $N = 2$, so there are $N + 1 = 3$ notches and therefore $N + 2 = 4$ slices on the top and the bottom sides respectively.

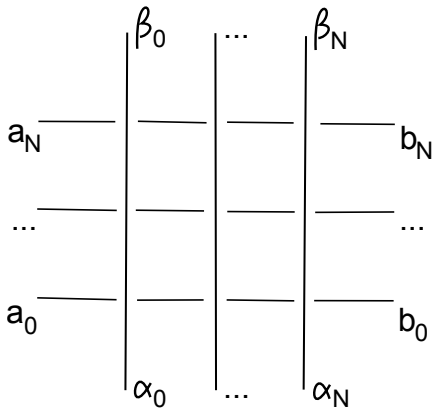

Figure 14 Sketch of the interior edges of the Chazelle polyhedron seen from above. In this picture $N = 2$.

The precise labels are given as shown in the following figures, where $i = 0, ..., N$ and $j \in \{-1, N + 1\}$:

(i) the ones in the interior part are $\alpha_i, \beta_i, a_i, b_i$ (see Figure 14),

(ii) the vertices on the top slices are labeled by $\alpha'_i, \alpha''_i, \alpha^*_j, \beta'_i, \beta''_i, \beta^*_j$ respectively (see Figure 15 left),

(iii) the ones on the bottom slices are $a'_i, a''_i, a^*_j, b'_i, b''_i, b^*_j$ (see Figure 15 right).

In Table 1 we give the sets of tetrahedra we remove from the Chazelle polyhedron to obtain the so called Reduced Chazelle polyhedron. For an easier imagination of the sets, we split them up into separate regions. The boundary slices A, B, C and D are sketched in Figure 16, they are labeled clockwise when seen from above.

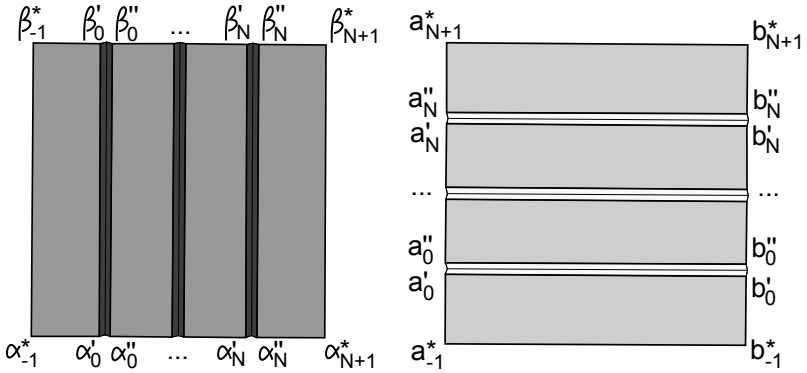

Figure 15 Left: top view on the slices of the Chazelle polyhedron, Right: view from the bottom. In this picture $N = 2$.

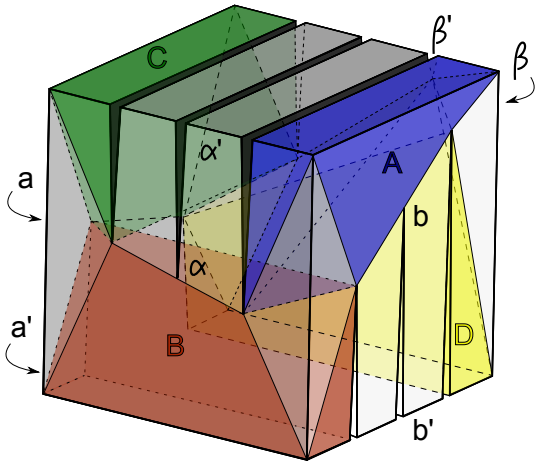

Figure 16 The Chazelle polyhedron with labeled boundary slices A-D. Only the interior edges of the polyhedron belonging to at least one of these slices are shown. In this picture $N = 2$.

Then, the corners are the connecting tetrahedra between these boundary slices. Therefore, there are four of them. We conclude with a way to tetrahedralize the slices on the top and bottom side, which are lying between the boundary slices. By construction, there are $N - 1$ of these interior slices on the top and bottom side respectively.

B Proof of Lemma 1

Each Steiner point $s_{i,j}$ has its coordinates $(i, j, ij + \omega)$. We can calculate the determinants directly. We show the calculation of equation (1), which is:

$$\det(s_{J+1,N+1-I}, s_{J,K-1}, s_{J+1,N-I}, s_{J,K}),$$

Boundary Slices	
(A)	$b_N\beta_N\alpha''_N\beta^*_{N+1}$ $\beta_N\alpha''_N\beta''_N\beta^*_{N+1}$ $b_N\alpha''_N\alpha^*_{N+1}\beta^*_{N+1}$ $b_N\alpha_N\beta_N\alpha''_N$ $b_ib_{i+1}\alpha_N\alpha^*_{N+1}$ $b_N\alpha_N\alpha''_N\alpha^*_{N+1}$
(B)	$a_0\alpha_i\alpha_{i+1}a^*_{-1}$ $b_0a'_0b'_0b^*_{-1}$ $\alpha_Na'_0a^*_{-1}b^*_{-1}$ $a_0\alpha_Na'_0a^*_{-1}$ $a_0b_0\alpha_Na'_0$ $b_0\alpha_Na'_0b^*_{-1}$
(C)	$a_0\alpha_0\beta'_0\alpha^*_{-1}$ $\alpha_0\alpha'_0\beta'_0\alpha^*_{-1}$ $a_0\beta'_0\alpha^*_{-1}\beta^*_{-1}$ $a_0\alpha_0\beta_0\beta'_0$ $a_ia_{i+1}\beta_0\beta^*_{-1}$ $a_0\beta_0\beta'_0\beta^*_{-1}$
(D)	$b_N\beta_i\beta_{i+1}b^*_{N+1}$ $a_Na''_Nb''_Na^*_{N+1}$ $\beta_0b''_Na^*_{N+1}b^*_{N+1}$ $b_N\beta_0b''_Nb^*_{N+1}$ $a_Nb_N\beta_0b''_N$ $a_N\beta_0b''_Na^*_{N+1}$

Corners	$\alpha_N\alpha^*_{N+1}b_0b^*_{-1}$ $\beta_Nb_N\beta^*_{N+1}b^*_{N+1}$ $a_0\alpha_0\alpha^*_{-1}a^*_{-1}$ $\beta_0\beta^*_{-1}a_Na^*_{N+1}$
Top Slice (i)	$\beta_{i+1}\alpha_i\alpha_{i+1}\beta'_{i+1}$ $\alpha_i\alpha'_{i+1}\alpha_{i+1}\beta'_{i+1}$ $\alpha_i\alpha'_{i+1}\beta'_{i+1}\alpha''_i$ $\beta_{i+1}\alpha_i\beta_i\alpha''_i$ $\beta_{i+1}\beta_i\beta''_i\alpha''_i$ $\beta_{i+1}\beta''_i\beta'_{i+1}\alpha''_i$
Bottom Slice (i)	$a_ia_{i+1}a'_{i+1}b_i$ $a_ia_{i+1}b_ia''_i$ $a''_ia'_{i+1}b_ib''_i$ $a_{i+1}b_{i+1}b'_{i+1}b_i$ $a_{i+1}b_ib'_{i+1}a'_{i+1}$ $b''_ib'_{i+1}b_ia'_{i+1}$

Table 1 The sets of tetrahedra to remove from the Chazelle polyhedron by taking the index i from 0 to $N-1$. The remaining part will be called the Reducted Chazelle, which is not tetrahedralizable.

which equals to

$$
\begin{aligned}
& \det \begin{pmatrix} J+1 & N+1-I & (J+1)(N+1-I)+\omega & 1 \\ J & K-1 & J(K-1)+\omega & 1 \\ J+1 & N-I & (J+1)(N-I)+\omega & 1 \\ J & K & JK+\omega & 1 \end{pmatrix} \\
= & \det \begin{pmatrix} 0 & 1 & J+1 & 0 \\ 0 & -1 & -J & 0 \\ J+1 & N-I & (J+1)(N-I)+\omega & 1 \\ J & K & JK+\omega & 1 \end{pmatrix} \\
= & \det \begin{pmatrix} 0 & 0 & 1 & 0 \\ 0 & -1 & -J & 0 \\ J+1 & N-I & (J+1)(N-I)+\omega & 1 \\ J & K & JK+\omega & 1 \end{pmatrix} \\
= & \det \begin{pmatrix} 0 & -1 & 0 \\ J+1 & N-I & 1 \\ J & K & 1 \end{pmatrix} \\
= & \det \begin{pmatrix} J+1 & 1 \\ J & 1 \end{pmatrix} \\
= & \ 1
\end{aligned}
$$

Next we show the calculation of equation (4), which is:

$\det(s_{N+1-I,J-1}, s_{K-1,J}, s_{N-I,J-1}, s_{K,J})$,

which equals to

$$
\begin{aligned}
& \det \begin{pmatrix} N+1-I & J-1 & (J-1)(N+1-I)+\omega & 1 \\ K-1 & J & J(K-1)+\omega & 1 \\ N-I & J-1 & (J-1)(N-I)+\omega & 1 \\ K & J & JK+\omega & 1 \end{pmatrix} \\
= & \det \begin{pmatrix} 1 & 0 & J-1 & 0 \\ -1 & 0 & -J & 0 \\ N-I & J-1 & (J-1)(N-I)+\omega & 1 \\ K & J & JK+\omega & 1 \end{pmatrix} \\
= & \det \begin{pmatrix} 1 & 0 & -1 & 0 \\ -1 & 0 & -J & 0 \\ N-I & J-1 & (J-1)(N-I)+\omega & 1 \\ K & J & JK+\omega & 1 \end{pmatrix} \\
= & -1 \times \det \begin{pmatrix} -1 & 0 & 0 \\ N-I & J-1 & 1 \\ K & J & 1 \end{pmatrix} \\
= & \times \det \begin{pmatrix} J-1 & 1 \\ J & 1 \end{pmatrix} \\
= & -1
\end{aligned}
$$

C The Definition of Generalised Chazelle Polyhedron

Formally, we define a *generalised Chazelle polyhedron*, $\Pi_{N_b,N_t,\varepsilon}$ as following: the set of vertices of $\Pi_{N_b,N_t,\varepsilon}$ are: $\{a_i, b_i, \alpha_j, \beta_j \mid i = 0, \ldots N_b, j = 0, \ldots, N_t\}$, where the vertices a_i's

and b_i's are on $z = xy$, and α_j's and β_j's are on $z = xy + \varepsilon$. Without loss of generality, assume $N_t \geq N_b$. Then

$$\alpha_j := (j, -1, -j + \varepsilon), \text{ and } \beta_j := (j, N_t + 1, j(N_t + 1) + \varepsilon);$$

and

$$a_i := (-1, -1{+}u{*}(i{+}1), 1{-}u{*}(i{+}1)), \text{ and } b_i := (N_t{+}1, -1{+}u{*}(i{+}1), (N_t{+}1){*}(-1{+}u{*}(i{+}1)));$$

where $u = \frac{N_t+2}{N_b}$.

The set of boundary faces of $\Pi_{N_b,N_t,\varepsilon}$ are:

(1) $\{\alpha_j\beta_j + 1\beta_j, \alpha_j\beta_j + 1\alpha_j + 1 \mid j = 0, \ldots, N_t - 1\}$;
(2) $\{\alpha_{N_t} b_i b_{i+1}, \beta_0 a_i a_{i+1} \mid i = 0, \ldots, N_{b-1}\}$;
(3) $\{a_{i+1} b_i a_i, a_{i+1} b_i b_{i+1} \mid i = 0, \ldots, N_b - 1\}$;
(4) $\{a_0\alpha_i\alpha_{i+1}, b_{N_b}\beta_i\beta_{i+1} \mid i = 0, \ldots, N_b - 1\}$;